Binder effects in photopolymerized acrylate/zeolite composites for 3D printing/ion-exchange applications

Yuanyuan Gao, Yijun Zhang, Laure Michelin, Jacques Lalevée, Angélique Simon-Masseron

Binder effects in photopolymerized acrylate/zeolite composites for 3D printing/ion-exchange applications

Yuanyuan Gao[1,2], Yijun Zhang[1,2], Laure Michelin[1,2], Jacques Lalevée[1,2*], Angélique Simon-Masseron[1,2*]

[1] Université de Haute-Alsace, CNRS, IS2M UMR 7361, F-68100 Mulhouse, France
[2] Université de Strasbourg, France

***Corresponding authors:**

Angélique Simon-Masseron, angelique.simon-masseron@uha.fr

Jacques Lalevée, jacques.lalevee@uha.fr

Abstract

In this paper, the influence of permanent binder was first determined on the photopolymerization process under mild condition (visible LED irradiation, at room temperature and under air) of LTA zeolite /polymer based composites. Different inorganic binders were tested in order to investigate their optical properties and to improve the mechanical properties after polymer removal by thermal treatment. Optimum formulation obtained with poly(ethylene glycol) diacrylate (PEGDA) and colloidal silica demonstrates excellent Depth of Cure (DOC) and good spatial resolution. The monolith obtained after thermal treatment at 600 °C shows hierarchical porosity with high BET surface area and high compressive strength. Furthermore, Ni^{2+} and Sr^{2+} ion exchange capacities were evaluated and the effect of colloidal silica as binder was investigated. This work extends our understanding of highly-filled composites (solid content up to 60.8 wt% where zeolite content = 40 wt%/21 vol%) obtained by photopolymerization, and expands their applications for 3D printing of high-performance lightweight materials and ion exchange.

Keywords

Polymer-matrix composite, mechanical properties, optical properties, porosity, 3D printing

1. Introduction

In recent years, additive manufacturing (AM), also known as 3D printing of composites is developing rapidly in academia and industry. Several AM technologies exist [1], the most common ones are: 1) Materials Extrusion (Fused deposition modeling), in which a material is selectively dispensed through a nozzle; 2) Vat Polymerization (Stereolithography, Digital light processing and Direct laser write), in which a photocurable polymer/composite is selectively cured by UV-vis light; 3) Powder Bed Fusion (Selective laser sintering, Direct metal laser sintering and Selective laser melting), in which a high-energy source selectively fuses powder particles; 4) Material Jetting, in which droplets of material are deposited and cured in desired form; 5) Binder Jetting, in which a liquid bonding agent selectively binds regions of powder bed. Compared to other technologies, 3D printing through photopolymerization represent advantages such as high production rate, mild reaction temperature, absence of volatile organic compounds (VOCs), low energy consumption, excellent spatial and temporal control, etc [2,3]. However, photopolymerization of highly filled polymers still faces its challenge, for the poor light penetration caused by absorption and scattering [4].

Zeolites are a set of crystallized aluminosilicates consisting of a framework based on three-dimensional structure of SiO_4 and AlO_4 tetrahedra molecules linked to each other by sharing oxygen. The existence of trivalent aluminum gives the framework negative charges which need to be compensated by extra-framework cations [5,6]. The general formula of zeolite can be written as

$M_{2/n}O.Al_2O_3.xSiO_2.yH_2O$, where 'x' is always equal to or greater than 2 and 'n' is the valence of the extra-framework cation 'M' [7]. The Si/Al ratio varied between 1, in type-A zeolite, and infinite in silicalite for example [8]. Linde Type A (LTA) zeolite is the most important class of small pore zeolite structure and was the first synthetic zeolite to be commercialized by Milton and co-workers in 1956 [9]. Depending on the compensation cation in the zeolite framework, it can be termed zeolite 3A, 4A or 5A when the cation is potassium, sodium or calcium respectively [10]. These microporous materials have a large fields of applications such as adsorption, gas separation, water treatment, ion exchange and catalysis [11–16].

In recent years, a lot of work combining porous materials as fillers with polymers were done to elaborate composites as 3D printing materials used in medicine industry [17,18], adsorption and separation industry [19–22]. Liu et. al. [17] incorporated Ag-carrying halloysite nanotubes (1-3 wt%) into a light-curing resin to prepare dental materials which has antibacterial property *via* DLP technique. Thakkar et. al. [22] fabricated composite monoliths consisting of zeolite 13X/5A (30 wt% in monolith, 13 wt% in dope composition) and Torlon polymer *via* robocasting (extrusion process) for the removal of CO_2 from the flue gas. Lefevere et. al. [23] studied the influence of binders in 3D printing *via* extrusion using ZSM-5 (65 wt% in monolith, 39-47 wt% in dope composition) as active material to build up the structured adsorbent/catalyst and bentonite, colloidal silica or aluminophosphate solution as binders. These compounds had an impact on the formulation properties and on the porosity and mechanical strength of monolith. In our previous work, we studied the photopolymerization kinetics and the depth of cure in zeolite/polymer system [24], the mechanical and functional properties (ca. gas adsorption) of composites (zeolite maximum content ~95 wt%) [25,26].

In this work, the development of zeolite-binder-polymer composites through photopolymerization was described. Binders were introduced in the formulation to increase mechanical properties of the composite before and after thermal treatment as well as to keep structure and physical-chemical properties of zeolite. PEGDA polymer was selected because of its biocompatibility, inexpensive cost, highly reactivity, commercial availability and it induces mild reaction condition (near room temperature and without intense heat releasing). After thermal treatment at 600 °C, PEGDA was removed and the zeolitic monolith retains the shape and porosity. The easy sample handling even after polymer removal represents a breakthrough in 3D printing for zeolite based composites and zeolite shaping. The viscosities of printing slurries were analyzed and the polymerization results were evaluated mainly through the depth of cure (DOC). Dynamic thermomechanical analysis (DMA) and thermogravimetric analyses (TGA) were performed on the composites before thermal treatment. Scanning electron microscopy (SEM), X-ray diffraction measurements (XRD), N_2 adsorption-desorption and compressive strength test were carried out on the calcined composites (monoliths). The ion exchange capacity of both composite and monolith were evaluated.

2. Experimental Section

2.1. Materials

The zeolite powder (LTA-5A) was purchased from Acros Organics and was dried at 80 ^{o}C overnight before use. The oligomer poly(ethylene glycol) diacrylate (PEGDA, Mw ≈ 600) was supplied by Sartomer (SR610). The photoinitiator 2-benzyl-2-(dimethylamino)-4'-morpholinobutyrophenone (BDMK-Irgacure® 369), the selected binders as kaolin, bentonite, montmorillonite K10, water glass (sodium silicate solution, 26.5 wt%

SiO_2, 10.6 wt% Na_2O) and colloïdal silica (LUDOX HS-40, 40 wt%) were obtained from Sigma-Aldrich. Other binders as fumed silica (Aerosil 150) and monoaluminium phosphate solution (Lithopix P1, 50 wt%) were purchased from Evonik and Zschimmer&Schwarz respectively. The chemical structures of oligomer and photoinitiator are listed in Scheme 1. Characteristics of zeolite are listed in Table S1.

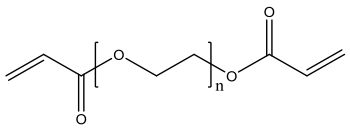

PEGDA

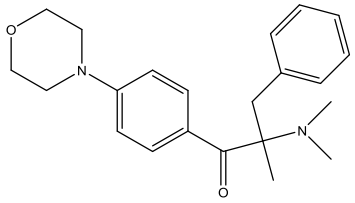

Irgacure 369

Scheme 1. Chemical structures of oligomer and photoinitiator used in this work

2.2. Sample preparation

Different stages of sample preparation are described in Scheme 2: 1 wt% of the photoinitiator (based on total weight of the formulation) was dissolved in the oligomer PEGDA. Then depending on the binder type, the printing slurries can be prepared in two different ways. For the powdery binder, namely bentonite, kaolin, fumed silica and montmorillonite, the binder was added together with zeolite into PEGDA and stirred with the Speedmixer (DAC 150.1 FVZ-K) until homogeneously dispersed mixtures were obtained. In contrast, liquid binder, such as water glass, colloidal silica, and lithopix P1, was added first to PEGDA. After stirring with Speedmixer, PEGDA was swelled up and the zeolite powder was then dispersed by Speedmixer. The slurries were preserved in dark place before use to prevent the decomposition of photoinitiator. The zeolite content was fixed at 40 wt% (corresponding to ~21% in volume) in this work in order to easily modify the content of binder and

to ensure the quantity of oligomer in the formulation for an efficient polymerization. The amount of binder was chosen depending on the amount of zeolite and presented in dry weight basis (dwb%). For example, the amount of colloidal silica is 30 dwb% when 75 g (0.75 g) of colloidal silica solution (40 wt%) is mixed with 100 g (1 g) of zeolite. To compare the DOC, 10 dwb% of different binders were added to the formulations whose compositions are reported in Table S2. Formulations were noted P-LTA-(binder with dwb% for colloidal silica).

The prepared formulation was transferred into a mold (rubber tube with opaque wall, one end opens to air and the other closed up with a cap) before irradiation with a LED lamp for 30 s (LED @ 405 nm; 1 W/cm^2). The cured composite was washed with acetone to remove the residual oligomers and heated at 80 °C overnight to evaporate acetone and residual water. This step is necessary to avoid cracks during the subsequent heat treatment.

Cured polymer-zeolite-binder composites were heated up to 600 °C under air with a temperature profile reported in Figure S1. After this thermal treatment (named t), the organic part (polymer) was removed while retaining the shape of the composite. The remaining inorganic objects were referred to as monoliths and were named P-LTA-dwb% silica (t).

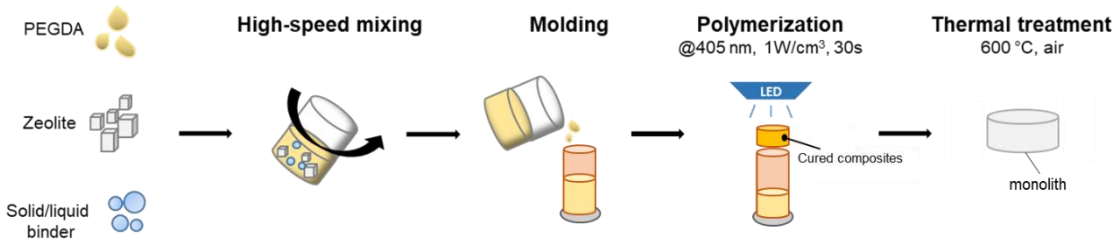

Scheme 2. Sample preparation process

2.3. Characterization Methods

Depth of cure (DOC) was measured by an Absolute LCD Digimatic Indicator (Mitutoyo) after irradiation for 30 s. Then composites were polished to obtain pellets with a thickness of 1 mm for Dynamic Thermomechanical Analysis (DMA) which were carried out on Viscoanalyser METTLER DMA861 at a frequency of 1.00 HZ in the tensile configuration at 25 °C. A rotational rheometer HAAKE MARS (Thermo Scientific) was used for the rheology measurements with a shear rates between 0.01 and 1000 s^{-1} at 25 °C. Thermogravimetric analyses (TGA) were recorded under air with a heating rate of 5 °/min from 30 to 800 °C on a METTLER-TOLEDO TGA/DSC 3+ thermoanalyzer. Compressive strength tests were performed on the monoliths (3 mm height and 9 mm diameter) by adding different weights (50-300 g) during 30 s. The homogeneity in the monolith and the morphology of inorganic particles were studied by scanning electron microscopy (SEM) using a JEOL JSM-7900F microscope. The accelerated volt-age used was 2 kV. Prior to the observations, all samples were coated with carbon.

The crystalline structure was identified by X-ray diffraction (XRD) measurements using a PANalytical MPD X'Pert Pro diffractometer operating with Cu Kα radiation (Kα = 0.15418 nm) equipped with an PIXcel real-time multiple strip detector (active length = 3.347 ° (2θ)). The powder patterns were collected in the range 3 ° < 2θ < 70 ° with a step of 0.013 ° (2θ) and a time/step equal to 220 s at 295 K. The patterns were analyzed by using the X'Pert HighScore software package and compared with data of the International Centre for Diffraction Data (ICDD) database.

Nitrogen (N_2) adsorption-desorption isotherms were performed on Micromeritics ASAP 2420 Instrument at -196 °C. Specific surface areas were calculated according to the Brunauer-Emmett-Teller (BET) method (relative pressure p/p° < 0.05) [27]. Prior to N_2 sorption measurement, samples were outgassed to a residual pressure of less than 0.8 Pa at 90 °C for 1 h and

300 °C for 15 h. The *t*-plot method using the Harkins-Jura thickness equation was used to determine the microporous volume (V_{micro}) and microporous surface area (S_{micro}). The external surface (S_{ext}) was obtained by subtracting S_{micro} from the total surface (S_{BET}). Mesopore size distributions were calculated by the BJH (Barrett-Joyner-Halenda) method on the desorption branch of the isotherm.

Elemental analyses were performed by X-Ray Fluorescence spectrometry (XRF) with a PANalytical Zetium (4 kW) spectrometer. Samples were mixed with boric acid and pressed into pellets of 13 mm diameter with 5 tons of pressure before the analysis.

^{27}Al MAS NMR spectra have been recorded on a Bruker Avance AVANCE NEO 400WB spectrometer (B_0 = 9,4T) operating at 104.23 MHz. Samples were packed in a 2.5 mm diameter cylindrical zirconia rotor fitted with Vespel end caps and spun at a spinning frequency of 25 kHz. ^{27}Al MAS NMR experiments were collected with a proton π/12-pulse duration and a recycle delay of 0.33 μs and 1 s, respectively. The number of accumulations varied from 50000 to 90000. The chemical shifts were referenced to $[Al(H_2O)_6]^{3+}$ in $AlCl_3$ aqueous solution (external reference).

2.4. Lithography Experiment and Water Swelling Test

Lithography experiment was performed in order to study the spatial resolution of the formulations. A computer-programmed laser diode (Thorlabs) with spot size around 50 μm was used to produce specific patterns from the photocurable composites which were deposited onto homemade resin tank (40×20×2 mm). The printed patterns were observed through a numerical optical microscope (DSX-HRSU, OLYMPUS Corp.).

Composites prepared in photolithography experiment were characterized for water swelling property. This is an important parameter because the ion exchange tests were realized in aqueous

solutions. Samples were submerged in distilled water and taken out periodically to weigh after the water on the surface of the samples was wiped out. A stable mass was obtained after several hours. The percentage of water swelling (water swelling rate) was calculated by equation (1):

$$X(\%) = \frac{m_2 - m_1}{m_1} \times 100 \quad (1)$$

with m_1 and m_2, mass of dry composite and stable mass of composite after water swelling, respectively.

2.5. Ion Exchange Tests

In order to determine the ion exchange ability of the photocured objects (before and after thermal treatment) and the influence of polymer and binder, Ni^{2+} and Sr^{2+} were chosen as they often present in industry or nuclear wastewater [11,28–32]. Some pellets (d = 9 mm, l = 3 mm) containing LTA as filler and silica as binder were obtained using a special mold as described in section 2.2

Sr^{2+} and Ni^{2+} adsorption was tested by soaking the pellets in 0.1 M $Sr(NO_3)_2$ or 0.1 M $Ni(NO_3)_2$ aqueous solution (pH approximately = 7) with V : m = 100 : 1 and 50 : 1 (mL : g) respectively during 24 h at room temperature under agitation (shaker, IKA HS 260 basic). A magnetic stirring was used for zeolite powders. After ion exchange, the pellets or powders were rinsed with ~50 mL of deionized water and dried at 80 °C overnight. The exchanged composites were calcined at 600 °C and ground to powders for XRD and XRF analyses.

The exchange rate was calculated and normalized to aluminum atoms from the equation (2) :

$$Exchange\ rate\ (\%) = \frac{2 \times n_{Sr\ or\ Ni}}{n_{Al}} \times 100 \quad (2)$$

with $n_{Sr\ or\ Ni}$ and n_{Al} the amount of Sr, Ni and Al respectively.

3. Results and Discussion

3.1. Depth of Cure

DOC is an important parameter in the study of photopolymerization reaction and its corresponding applications such as 3D printing. In this work, the DOC is defined as the thickness of materials cured adequately after exposition under visible light @ 405 nm for 30 s with an irradiation dose of 30 J/cm^2. In our previous works, it has been shown that DOC depends on the type and content of the fillers, also on the photoinitiator and monomer [25]. Among all these parameters, the optical property of the fillers is of great importance. Light transmittance of filled system can be influenced by the refractive index mismatch between polymer and filler [33], also the morphology and size of the filler particle, which will result in different light absorption and scattering.

The use of inexpensive inorganic binders such as SiO_2, Al_2O_3 and clay are very common in industrial processes during zeolite shaping. Binders enhance the physical strength of zeolite monolith, and several studies report that zeolite-binder interactions can influence the reactivity, selectivity and stability of the overall material leading to (non-)covalent interaction and cation migration [34][35]. The purpose of this section is to investigate the light attenuation caused by the binders and its effect on the final results of photopolymerization. Therefore, DOC values were measured for formulations containing 40 wt% of LTA and 10 dwb% of different binders. As shown in Figure 1a, pure PEGDA presents very good light penetration at 405 nm and resulted in excellent depth of cure (ca. 13 mm). The addition of LTA zeolite (binderless) caused strong light attenuation through the resin and reduced DOC drastically due to the light scattering. Binders of clay type (bentonite, kaolin and montmorillonite) induced a further decrease of the DOC as their bidimensional structure and relatively large particle size (> 10 μm) may increase the light absorption

and scattering, which resulted in more optical losses [36]. Nano-sized fumed silica, with its extremely low bulk density and high surface area induced by nanoparticle size, didn't have a significant impact on the DOC when using the tested concentration. Finally, unlike phosphate binder (Lithopix P1), silicate liquid binders (water glass and colloidal silica) improved the DOC when adding a small amount. The higher performance with colloidal silica may be related to the nano particles size (~20 nm) which was much below the wavelength (405 nm), resulting in Rayleigh Scattering and improving light penetration in the mixture [37]. So far colloidal silica (10 dwb%) increased the value of the DOC by 22 % but the positive effect disappeared when colloidal silica content increased (Figure 1b), possibly because of the intense growth of viscosities (section 3.2).

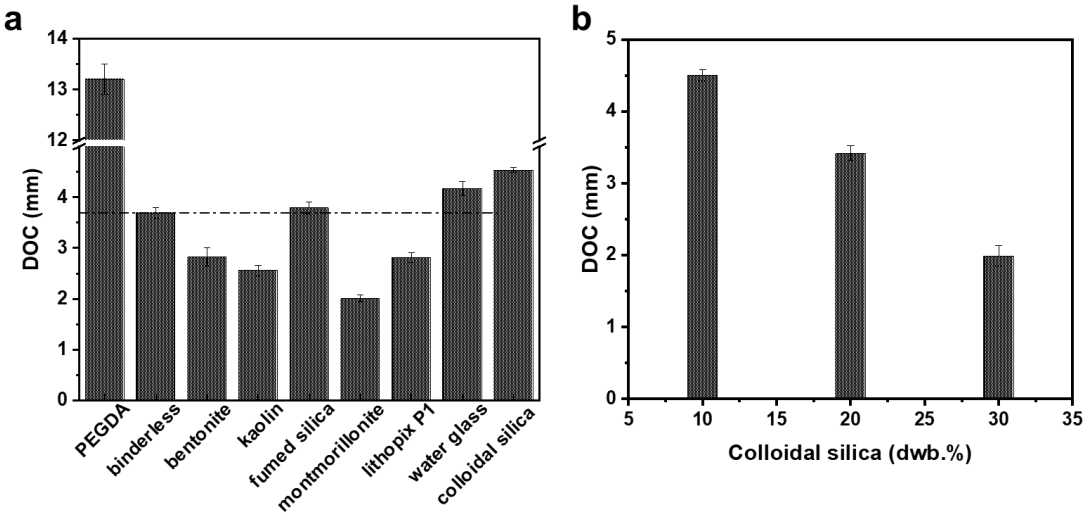

Figure 1. (a) DOC for pure PEGDA and formulations containing 40 wt% of LTA with 10 dwb% of different binders, (b) DOC for formulations containing 40 wt% of LTA with 10, 20, 30 dwb% of colloidal silica.

3.2. Viscosities

Viscosity of PEGDA oligomer and formulations with 40 wt% zeolite loading with silica content of 0, 10, 30 dwb% were measured at different shear rates (Figure 2). The oligomer PEGDA had very

low viscosity. Once adding zeolite, the viscosity increased and was more than 2 orders of magnitude higher at low shear rate (1 order at high shear rate). The addition of nano-sized silica resulted in surface roughness so that the result of formulations with 10 and 30 dwb% may not be representative. However, the formulations became more viscous indeed as the solid content increased after adding silica and the non-Newtonian fluid properties were enhanced.

All formulations exhibited shear thinning property which can be potentially used in deposition technique. However, high viscosity could hinder the diffusion of monomers in the reaction medium and reduce the reaction rate, resulting in poor depth of cure for formulations with high silica content.

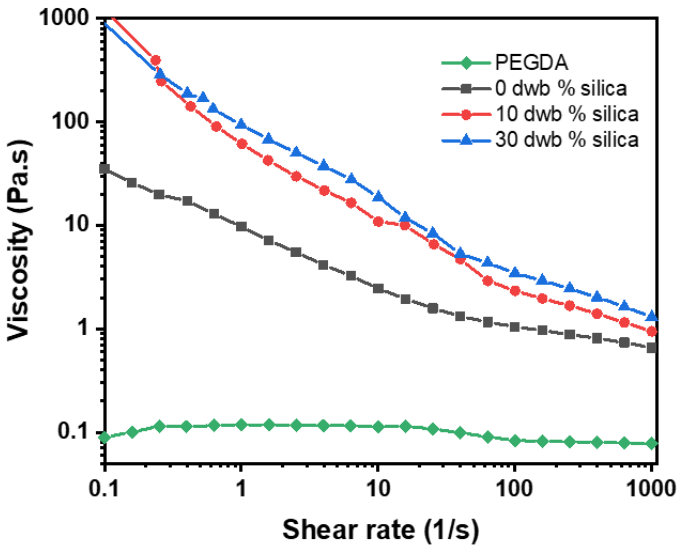

Figure 2. Viscosity curves for formulations containing 40 wt% of LTA and various amount of silica from colloidal silica.

3.3. Mechanical Properties

DMA tests were carried out on the composite pellets before thermal treatment. The storage modulus (G') is proportional to the stored energy which characterizes the elastic behavior of the material. The loss modulus (G") on the other hand, represents the viscous portion of the material.

Compared to the pure PEGDA polymer, the elastic modulus (G') after zeolite addition has increased by 291% (Figure 3), indicating a much stronger resistance to elastic deformation. It was further increased by adding at least 20 dwb% silica as the presence of sufficient small solid particles can increase the constraints of segmental motions in polymer networks. With only 10 dwb% silica, the space between particles was too large to interact with each other. The results were reproducible indicating that the binder particles were in strong polymer interactions and homogenously dispersed.

As DMA tests cannot be realized on the monoliths, the mechanical properties of them were evaluated *via* compressive strength tests (Figure S2). The minimum weights needed to crack the pellets are reported in Table 1. The P-LTA (t) sample was very difficult to handle after thermal treatment indicating that the binding strengths were not strong enough with only 40 wt% of zeolites as filler. With the addition of colloidal silica, monoliths became much harder and easier to handle. Silica particles may interact with filler particles inducing an increase of the mechanical strength.

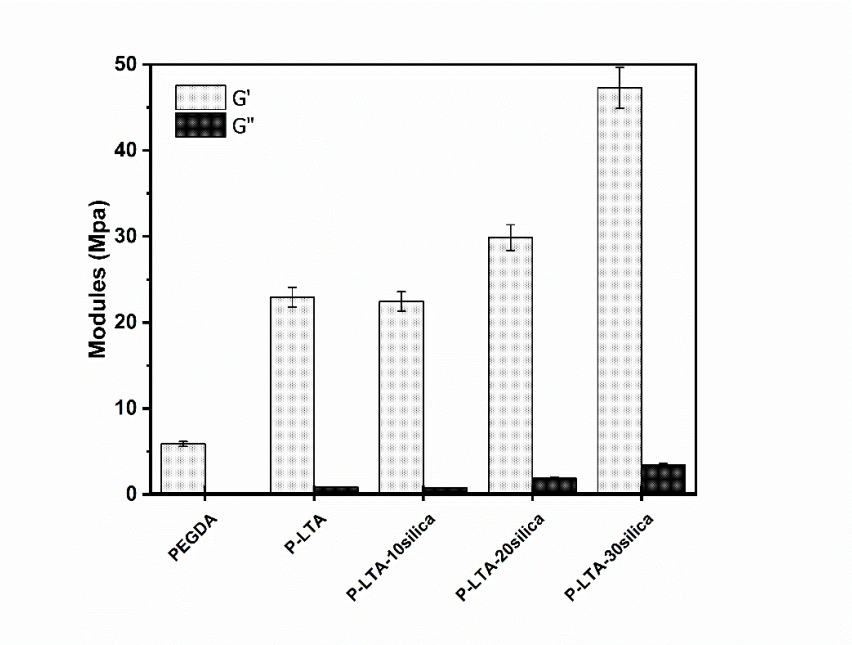

Figure 3. DMA results for pure PEGDA polymer, P-LTA and P-LTA-10/20/30silica composites.

Table 1. Compressive strength test on monolith pellets after thermal treatment at 600 °C

	Minimum weight to break the monolith	Comment
P-LTA (t)	< 50 g	Very difficult sample handling
P-LTA-10silica (t)	100 g	Possible to handle
P-LTA-20silica (t)	300 g	Easy sample handling
P-LTA-30silica (t)	> 300 g	Easy sample handling

3.4. Thermal Analysis of Composites

The thermal behavior of composites was observed by thermogravimetric analyses (figure 4). The first weight loss observed until 200°C was associated to water desorption from zeolite. Between 200°C and 550°C, PEGDA decomposed. 32.4, 39.2, 45.1 and 53.7 wt% of composites were recovered for samples prepared with 0, 10, 20 and 30 dwb% of silica in theory (figure 4a). Thus, zeolite content in the monoliths can be calculated as 82.6, 71.8 and 60.3 wt% for P-LTA-10silica(t), -20silica(t) and -30silica(t) respectively. These values are higher than the theoretic ones because the water from colloidal silica could evaporate during photopolymerization (exothermic) and before the TG analysis, resulting in higher solid content. As observed on figure 4b, the presence of zeolite lowered ca. 50°C the temperature of PEGDA decomposition. The influence of binder doesn't seem

to be solely related to its amount.

The results indicate that the calcination temperature (600 ^{o}C) is suitable to remove the polymer from the composite, as the weight loss of pure PEGDA achieved 100%. At this temperature, textural characteristics of the zeolite should not be significantly affected as further proved by N_2 adsorption-desorption experiment.

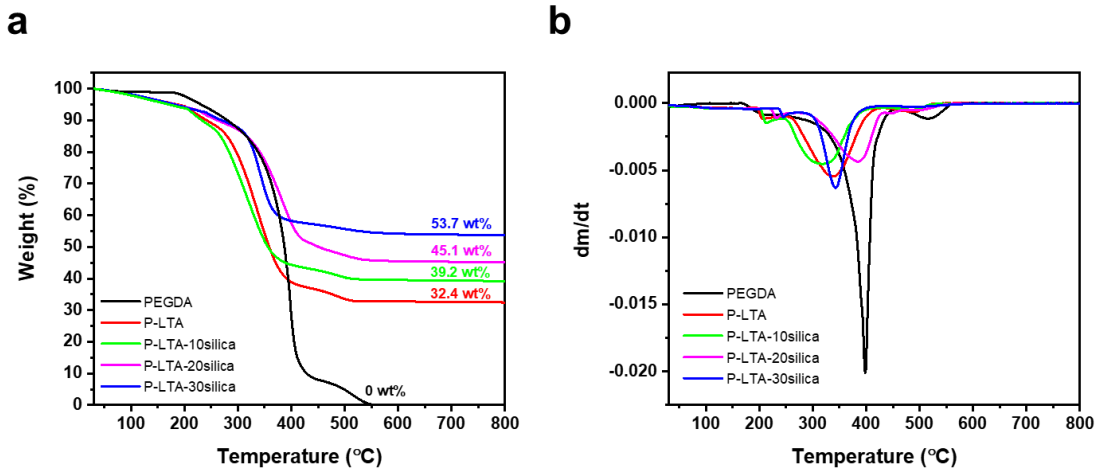

Figure 4. (a) TGA and (b) its derivative (DTG) for PEGDA polymer, P-LTA and composites with respectively 10, 20 and 30 dwb% of silica.

3.5. Spatial Resolution and Water Swelling Property

The laser write experiments were performed at 405 nm for formulations containing 40 wt% LTA with respectively 0, 10, 20, 30 dwb% of silica in order to study the spatial resolution. As shown in Figures 5, LTA based composites have high reactivity allowing a very efficient photocuring in the irradiated area with patterns up to ~2 mm thickness in a short printing time (<1 min for a 2 cm length pattern). The addition of silica affected the light scattering and therefore influenced the light penetration in the formulation, resulting in less good resolution compared to the composite containing only zeolite, especially for those with lower binder contents. Furthermore, we observed

that the shrinkage reduced while increasing solid content, as the letters became thicker (figure 5, column b from top to bottom).

Water swelling tests were carried out using the same samples prepared from lithography experiment. The pictures of the composites with different content of silica before and after water sorption as well as after water removal at 80 ^{o}C are reported in Figure 5c. PEGDA polymer is known for its water swelling property, which can take water up to 85% of its own weight [25]. It was observed that the 3D patterns (letter "D") expanded in volume after water sorption and returned to the origin size after water removal. This process was completely reversible. As shown in Figure 6, when adding 10 dwb% of silica, the water swelling rate decreased by 20% compared to that of composite containing only LTA. However, when increasing the silica content in the range of 10-30 dwb%, water swelling rate kept relatively stable. Some samples with relatively low solid content generated cracks on the surface after water sorption, it may be caused by the poor mechanical property obtained from PEGDA polymer after polymerization (section 3.3) that the macromolecular chains cracked during volume expansion. When the solid content reaches a certain level, the constraint of segmental motions in polymer network is strong enough to avoid cracks.

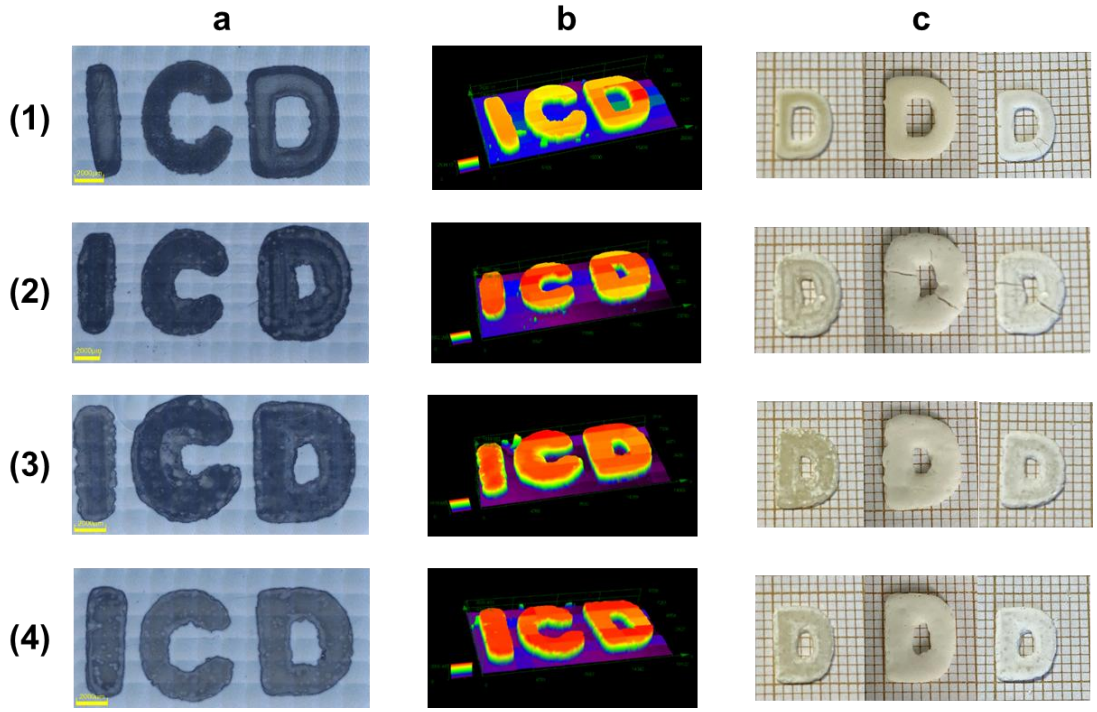

Figure 5. Laser write at 405 nm from (1) P-LTA, (2) P-LTA-10silica, (3) P-LTA-20silica and (4) P-LTA-30silica with 0.05 wt% BDMK and characterized by a numerical optical microscopy: (a) top surface morphology, (b) color patterns (colors represent the thickness) and (c) photos of water swelling experiments: left – before water sorption; middle – after water sorption; right – after water removal.

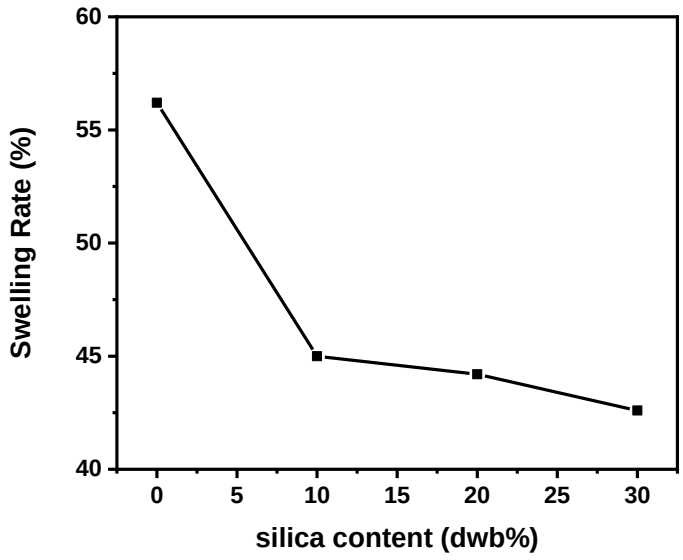

Figure 6. Water swelling property of composites containing 40 wt% LTA with 0, 10, 20, 30 dwb% of silica (polymer: PEGDA; photoinitiator: BDMK; photopolymerization @ 405nm).

3.6. Structural and microscopic characterization of monoliths

Monoliths were analyzed by XRD in order to control the thermal stability of zeolite. All XRD patterns are similar to pattern of the pristine LTA powder (Figure S3). They show the diffraction peaks typical of the LTA topology with a cubic unit cell. The lattice parameters were calculated and variations of less than 0.1% were observed between different crystallographic parameters (Table S3). Thus zeolite remained stable after calcination. Its structure was not affected by the small amount of amorphous silica binder detected from a broad bump around $2\theta = 25°$ [38,39].

Without binder, the surface of P-LTA (t) sample consists of an assembly of zeolite crystals with smooth faces and characterized by a cubic morphology with an average crystal size about 2 μm (Figure 7). No trace of PEGDA polymer was observed in agreement with the TG analysis. When 10 dwb% of colloidal silica was added, the surface of LTA crystal was covered by a thin layer of silica nanoparticles whose content increases logically with the amount of silica. As observed on TEM images (figure 7c), these particles are spherical (22 nm of diameter) and well dispersed in monolith. Figure 7b shows that they completely covered the zeolite crystals and bind them together. It could explain the increase of the mechanical properties when increasing the silica content (section 3.3, figure S2). A good dispersion of zeolite and binder as silica nanoparticles is of great importance because, as reported in the literature, homogeneously dispersed fillers in the polymer matrix can improve hardness, strength, radiopacity and decrease the polymerization shrinkage, thermal expansion and contraction, and water sorption [40]. In addition to N_2 adsorption-desorption

experiments, SEM analyses highlight particle agglomeration during the thermal treatment to form macroporosity (pore diameter ≥ 50 nm) with macropores of inhomogeneous size and shape.

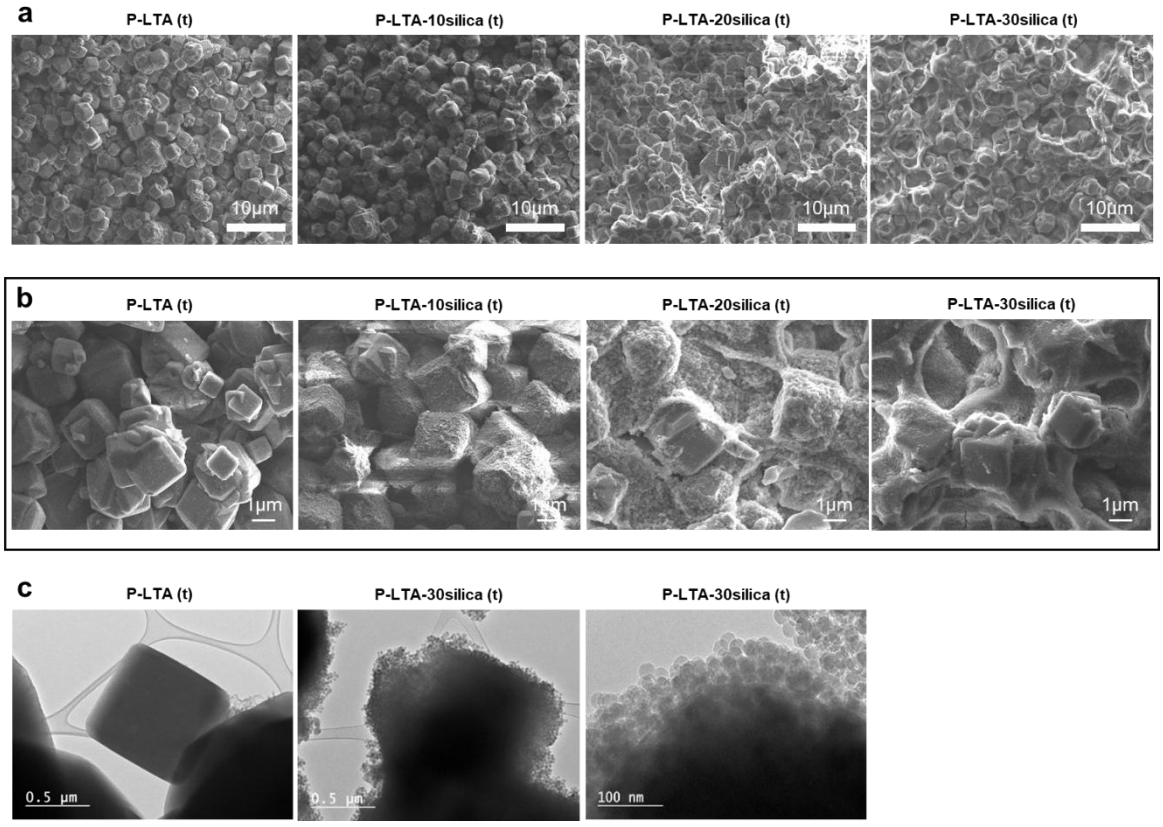

Figure 7. SEM and TEM images of the cross section of monoliths after thermal treatment with varying silica contents: (a) SEM: 2500×; (b) SEM: 10000×; (c) TEM

3.7. N_2 Adsorption-Desorption Isotherms

Textural properties of monoliths were evaluated by nitrogen adsorption-desorption. As reported on Figure 8, no obvious difference was observed between zeolite powder and P-LTA (t) sample, indicating that the thermal treatment did not significantly affect the textural properties of zeolite. The corresponding isotherms are type I characteristic of microporous solids [41].

The use of colloidal silica as binder introduced mesoporosity to the monoliths as the external surface (S_{ext}) increased. Indeed, a colloidal silica sample dried over night at 80 °C (amorphous silica)

is characterized by type IV isotherms characteristic of mesopores with ink bottle geometry (H2a hysteresis loop) and 5.6 nm pores size (Table 2, Figure 8a). This mesoporosity was logically observed for monoliths containing silica as binder at ca. $0.3 < p/p^0 <$ ca. 0.7. It became minority compared to interparticle mesoporosity (observed for ca. $0.7 < p/p^0$) associated to pore size of ca. 10 nm.

The microporous surface (S_{micro}) and microporous volume (V_{micro}) reported by gram of dehydrated monoliths in Table 2 logically decrease with the increase of the binder. V_{micro} characterizes the quantity of accessible micropores in the materials. The values related to the amount of dehydrated zeolite (dz) became 0.26, 0.25, 0.23 for P-LTA-10silica(t), -20silica(t) and -30silica(t) respectively (calculated according to the water content in zeolite obtained from TGA). The decrease of the microporous volume compared to 0.29 $cm^3.g_{dz}^{-1}$ value associated to the pristine LTA meant that the presence of silica particles partially blocked the micropores of zeolite.

Zeolite retained its high textural properties after the thermal treatment but a part of the micropores is blocked in presence of nano silica particles. Monoliths with hierarchical porosity structure can be of great interests for adsorption application.

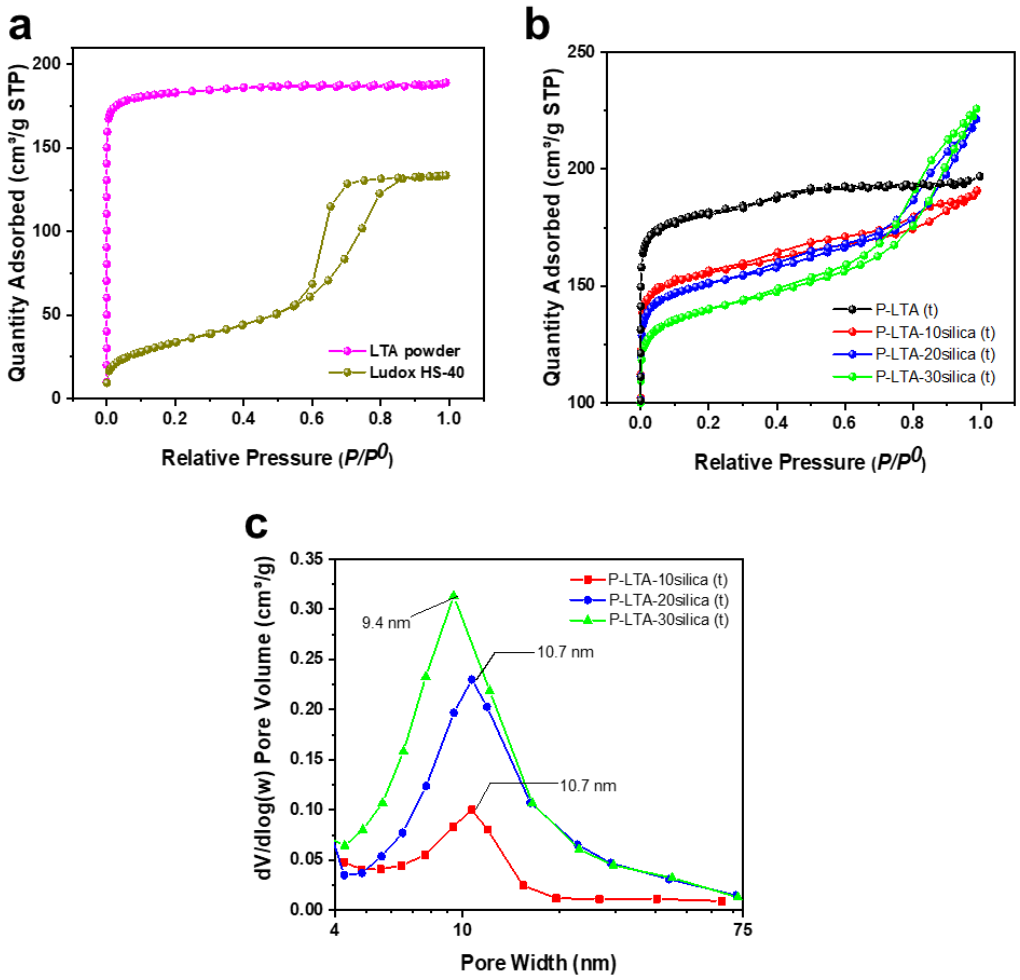

Figure 8. N_2 isotherms for (a) LTA powder and dry silica powder obtained from Ludox HS-40, (b) Composites of P-LTA, P-LTA-10silica, P-LTA-20silica and P-LTA-30silica after thermal treatment, and (c) mesopore size distribution for samples containing silica.

Table 2. Textural properties of pristine LTA powder, silica powder* and different monoliths determined by N_2 adsorption-desorption.

	S_{BET} ($m^2 \cdot g^{-1}$)	S_{micro} ($m^2 \cdot g^{-1}$)	S_{ext} ($m^2 \cdot g^{-1}$)	V_{micro} (cm^3/g)	V_{micro} (dz) (cm^3/g)	Pore diameter (nm)
LTA powder	747	744	3	0.29	0.29	< 2
Silica powder from Ludox HS-40*	123	6	117	0	/	5.6
P-LTA (t)	728	720	8	0.29	0.29	< 2
P-LTA-10silica (t)	620	582	38	0.23	0.26	10.7
P-LTA-20silica (t)	599	529	70	0.20	0.25	10.7
P-LTA-30silica (t)	549	451	98	0.17	0.23	9.4

*Evaporation of water under 80 ^{o}C during one night.

3.8. Ion Exchange Capacity

Ion exchange capacity of composites and monoliths were determined with Sr^{2+} and Ni^{2+} cations taking into account that the adsorption capacity of the cured PEGDA polymer is negligible (< 0.4 wt%, Table S4). Moreover, since the ion exchangers used in the nuclear industry are immobilized rather than regenerated or reused to avoid risk of spreading the hazards, the ion exchange experiments in our work were done for only one circle.

After an exchange of 24 h, composites and monoliths only with the highest silica content could keep their shape (Figure S7). Therefore, ion exchange experiments were focused on composites: P-LTA, P-LTA-30silica and monolith: P-LTA-30silica (t). Pristine powder was used as a reference.

As reported in Figure 9, the ion exchange kinetic was faster with Sr^{2+} than Ni^{2+} because they have different exchange mechanism. The uptake of Sr^{2+} is typical ion exchange determined by the zeolite framework composition. On the other hand, the uptake of Ni^{2+} depends more on the pore geometry due to the formation of phyllosilicate nanosheet [42]. Moreover, extra-framework aluminum created during Ni^{2+} exchange (Figure S5) may also limit the diffusion in micropores. The lattice parameters were similar to pristine powder after exchange (Figure S4, Table S5). But a peak splitting was observed in XRD with the nickel which could be explained by dealumination induced during exchange processes [43–46] highlighted by ^{27}Al NMR (Figure S5) and by the XRD pattern overlay of a dealuminated LTA sample (Figure S6).

Ion exchange capacity decreased with the following order whatever the cation: LTA powder > P-LTA30silica (t) > P-LTA30silica > P-LTA. For Sr^{2+} ion, the molar ratio Sr/Al was 0.24 for the pristine powder and 0.22 for the monolith with silica (P-LTA-30silica (t)). This small decrease of 8% can be explained by the fact that the presence of silica partially blocked the micropores of zeolite (section 3.7). The exchange rate of P-LTA composite dropped by 50% compared to the pristine powder. This is due to the presence of polymer that greatly limited cations diffusion and blocked micropores access. The presence of binder (P-LTA-30silica) seems slightly improved the exchange (only -33.3%) because the proton of silanol groups on the surface of silica particles can also exchange with cations [47].

For Ni^{2+} ion, the exchange rate for pristine powder after 24 h was 34.7%. This rate decreased by 64.7%, 58.8% and 52.9% for P-LTA, P-LTA-30silica and P-LTA-30silica (t) respectively. This decrease was mainly due to diffusional limitations in the presence of polymer for P-LTA and P-LTA-30silica composites and the formation of phyllosilicate that inhibited the access to

micropores for P-LTA-30silica (t).

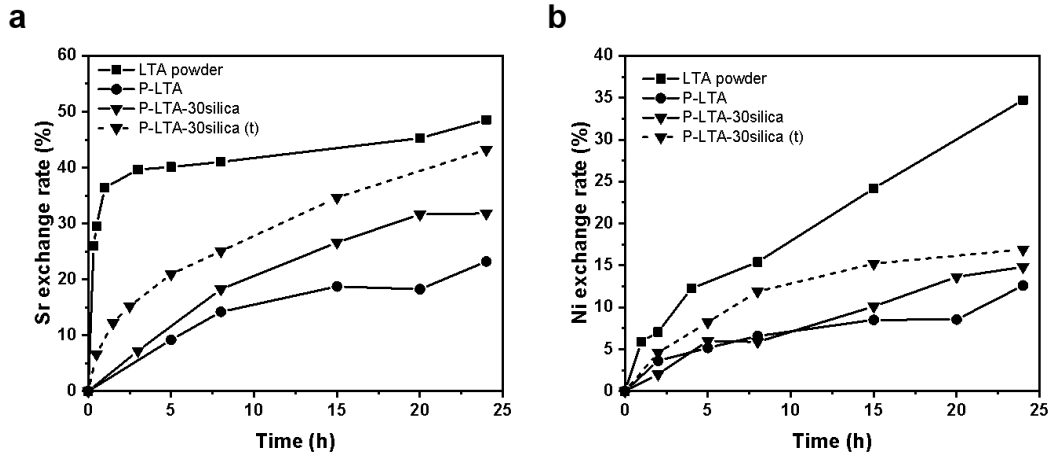

Figure 9. Exchange rate with LTA powder, P-LTA, P-LTA-30silica and P-LTA-30silica (t) for (a) Sr^{2+} and (b) Ni^{2+}.

After one day, the maximum of cationic exchange capacity was not reached. However, extrapolation of date suggests a small increase in nickel exchange capacity for monolith and composites in contrast to powder for time longer than 24h. The extrapolation leads to a slightly different conclusion with strontium. The cationic exchange capacity seems to be able to increase significantly beyond 24h for monolith.

Table 3. Elemental composition of LTA powder, composites and monoliths after an ion exchange of 24h.

	Before ion exchange		Sr exchanged		Ni exchanged	
Element	wt%	Atomic ratio	wt%	Atomic ratio	wt%	Atomic ratio
LTA powder						
Sr			14.07	0.24		
Ni					7.21	0.17
Al	19.75	1	17.85	1	19.10	1
Si	19.91	0.97	18.45	0.99	19.15	0.96
Ca	10	0.34	5.24	0.2	5.7	0.2
Na	4.07	0.24	1.76	0.12	3.89	0.24
	(Na + 2Ca)/Al = 0.92		(Na + 2Ca + 2Sr)/Al = 1.01		(Na + 2Ca + 2Ni)/Al = 0.98	
P-LTA						
Sr			7.32	0.12		
Ni					2.72	0.06
Al	5.46	1	19.51	1	20.21	1
Si	5.77	1.02	19.16	0.94	19.81	0.94
Ca	3.14	0.34	7.40	0.26	5.8	0.28
Na	2	0.4	1.92	0.12	3.91	0.23
	(Na + 2Ca)/Al = 1.08		(Na + 2Ca + 2Sr)/Al = 0.88		(Na + 2Ca + 2Ni)/Al = 0.91	
P-LTA-30silica						
Sr			6.94	0.16		
Ni					2.14	0.07
Al	13.57	1	13.44	1	13.28	1
Si	27.63	1.96	27.13	1.94	27.45	1.99
Ca	7.4	0.36	4.92	0.25	4.93	0.25
Na	3.25	0.28	0.8	0.07	4.06	0.36
	(Na + 2Ca)/Al = 1.03		(Na + 2Ca + 2Sr)/Al = 0.89		(Na + 2Ca + 2Ni)/Al = 1	
P-LTA-30silica (t)						
Sr			8.98	0.22		
Ni					2.45	0.08
Al	13.57	1	12.8	1	13.32	1
Si	27.63	1.96	25.98	1.95	27.72	2
Ca	7.4	0.36	4.71	0.24	4.87	0.24
Na	3.25	0.28	1.30	0.12	3.83	0.34
	(Na + 2Ca)/Al =1		(Na + 2Ca + 2Sr)/Al = 1.04		(Na + 2Ca + 2Ni)/Al = 0.98	

4. Conclusion

In this work, we have successfully prepared highly filled composites (up 60.8 wt%) with high zeolite content (> 21% in volume) at 405 nm LED irradiation under mild conditions by using high content of colloidal silica (30 dwb%). Zeolite crystals and silica nanoparticles were well dispersed, and monoliths with hierarchical structure and easy sample handling were obtained after thermal treatment at 600 ^{o}C.

The addition of silica particles greatly improved the mechanical properties for both composites and monoliths. After thermal treatment, silica particles partially blocked micropores of zeolite but provided silanol groups involved in ion-exchange with cations. Therefore, both PEGDA-LTA-silica composites and monoliths, which are more easily handled than powder, have potential applications in ion exchange for water decontamination for example. They are more effective with strontium than nickel. Moreover, the high resolution of the highly filled printing slurries by direct laser write could make it possible to design cured composites with complex shapes and then to obtain zeolitic monoliths with hierarchical porosity after thermal treatment. To our best knowledge, this is the first time that monoliths (after thermal treatment) could be used for ion exchange after shaping by photopolymerization.

This work finally expands our understanding about photopolymerization of highly filled polymer-based composite and contributes to the development of a new zeolite shaping process.

Conflicts of interest

There are no conflicts of interest to declare.

Acknowledgement

We thank Ludovic Josien, Gautier Schrodj and Habiba Nouali for their help concerning the SEM, DMA and nitrogen adsorption analyses respectively.

Reference

[1] M.D. Monzón, Z. Ortega, A. Martínez, F. Ortega, Standardization in additive manufacturing: activities carried out by international organizations and projects, International Journal of Advanced Manufacturing Technology. 76 (2015) 1111–1121.

[2] N. Corrigan, J. Yeow, P. Judzewitsch, J. Xu, C. Boyer, Seeing the Light: Advancing Materials Chemistry through Photopolymerization, Angewandte Chemie. 131 (2019) 5224–5243.

[3] C. Dietlin, S. Schweizer, P. Xiao, J. Zhang, F. Morlet-Savary, B. Graff, J.P. Fouassier, J. Lalevée, Photopolymerization upon LEDs: New photoinitiating systems and strategies, Polym Chem. 6 (2015) 3895–3912.

[4] Y. Zhang, Y. Xu, A. Simon-Masseron, J. Lalevée, Radical photoinitiation with LEDs and applications in the 3D printing of composites, Chem Soc Rev. 50 (2021) 3824–3841.

[5] S. Wang, Y. Peng, Natural zeolites as effective adsorbents in water and wastewater treatment, Chemical Engineering Journal. 156 (2010) 11–24.

[6] E. Kianfar, S. Hajimirzaee, S. mousavian, A.S. Mehr, Zeolite-based catalysts for methanol to gasoline process: A review, Microchemical Journal. 156 (2020).

[7] S. Kesraoui-Ouki, C.R. Cheeseman, R. Perry, Natural Zeolite Utilisation in Pollution Control: A Review of Applications to Metals' Effluents, J. Chem. Tech. Biorechnol. 59 (1994) 121–126.

[8] P. Sharma, M.H. Han, C.H. Cho, Synthesis of zeolite nanomolecular sieves of different si/al ratios, J Nanomater. 2015 (2015).

[9] D.W. Breck, W.G. Eversole, Milton R. M., New synthetic crystalline zeolites, J Am Chem Soc. (1956).

[10] F. Collins, A. Rozhkovskaya, J.G. Outram, G.J. Millar, A critical review of waste resources, synthesis, and applications for Zeolite LTA, Microporous and Mesoporous Materials. 291 (2020).

[11] M. Hong, L. Yu, Y. Wang, J. Zhang, Z. Chen, L. Dong, Q. Zan, R. Li, Heavy metal adsorption with zeolites: The role of hierarchical pore architecture, Chemical Engineering Journal. 359 (2019) 363–372.

[12] Q. Meng, H. Chen, J. Lin, Z. Lin, J. Sun, Zeolite A synthesized from alkaline assisted pre-activated halloysite for efficient heavy metal removal in polluted river water and industrial wastewater, J Environ Sci (China). 56 (2017) 254–262.

[13] K. Kawahara, K. Tsuruda, M. Morishita, M. Uchida, Antibacterial effect of silver-zeolite on oral bacteria under anaerobic conditions, Dental Materials. 16 (2000) 452–455.

[14] Ralph T. Yang, ADSORBENTS: FUNDAMENTALS AND APPLICATIONS, Wiley-Interscience, 2003.

[15] A. Huang, N. Wang, J. Caro, Synthesis of multi-layer zeolite LTA membranes with enhanced gas separation performance by using 3-aminopropyltriethoxysilane as interlayer, Microporous and Mesoporous Materials. 164 (2012) 294–301.

[16] Z. Wu, S. Goel, M. Choi, E. Iglesia, Hydrothermal synthesis of LTA-encapsulated metal clusters and consequences for catalyst stability, reactivity, and selectivity, J Catal. 311 (2014) 458–468.

[17] L. Sa, L. Kaiwu, C. Shenggui, Y. Junzhong, J. Yongguang, W. Lin, R. Li, 3D printing dental composite resins with sustaining antibacterial ability, J. Mater. Sci. 54 (2019) 3309–3318.

[18] Y. Qing, K. Li, D. Li, Y. Qin, Antibacterial effects of silver incorporated zeolite coatings on 3D printed porous stainless steels, Mater. Sci. Eng. C. 108 (2020).

[19] V. Middelkoop, K. Coenen, J. Schalck, M. van Sint Annaland, F. Gallucci, 3D printed versus spherical adsorbents for gas sweetening, Chemical Engineering Journal. 357 (2019) 309–319.

[20] H. Zhang, P. Wang, H. Zhang, H. Yang, H. Wang, L. Zhang, Structured Zeolite Monoliths with Ultrathin Framework for Fast CO2 Adsorption Enabled by 3D Printing, Ind. Eng. Chem. Res. 59 (2020) 8223–8229.

[21] H. Thakkar, S. Eastman, A. Hajari, A.A. Rownaghi, J.C. Knox, F. Rezaei, 3D-Printed Zeolite Monoliths for CO2 Removal from Enclosed Environments, ACS Appl. Mater. Interfaces. 8 (2016) 27753–27761.

[22] H. Thakkar, S. Lawson, A.A. Rownaghi, F. Rezaei, Development of 3D-printed polymer-zeolite composite monoliths for gas separation, Chem. Eng. J. 348 (2018) 109–116.

[23] J. Lefevere, L. Protasova, S. Mullens, V. Meynen, 3D-printing of hierarchical porous ZSM-5: The importance of the binder system, Mater. Des. 134 (2017) 331–341.

[24] Y. Xu, C. Jambou, K. Sun, J. Lalevée, A. Simon-Masseron, P. Xiao, Effect of Zeolite Fillers on the Photopolymerization Kinetics for Photocomposites and Lithography, ACS Appl Polym Mater. 1 (2019) 2854–2861.

[25] Y. Zhang, L. Josien, J.P. Salomon, A. Simon-Masseron, J. Lalevée, Photopolymerization of Zeolite/Polymer-Based Composites: Toward 3D and 4D Printing Applications, ACS Appl. Polym. Mater. 3 (2021) 400–409.

[26] Y. Zhang, Y. Gao, L. Josien, H. Nouali, C. Vaulot, A. Simon-Masseron, J. Lalevée, Photopolymerization of Zeolite Filler-Based Composites for Potential 3D Printing Application and Gas Adsorption Applications, Adv. Mater. Technol. 2100869 (2021) 1–11.

[27] M. Thommes, K. Kaneko, A. v. Neimark, J.P. Olivier, F. Rodriguez-Reinoso, J. Rouquerol, K.S.W. Sing, Physisorption of gases, with special reference to the evaluation of surface area and pore size distribution (IUPAC Technical Report), Pure and Applied Chemistry. 87 (2015) 1051–1069.

[28] L. Liu, K. Zhang, Nanopore-Based Strategy for Sequential Separation of Heavy-Metal Ions in Water, Environmental Science & Technology. 52 (2018) 5884–5891.

[29] S. sen Gupta, K.G. Bhattacharyya, Kinetics of adsorption of metal ions on inorganic materials: A review, Adv Colloid Interface Sci. 162 (2011) 39–58.

[30] W. Qiu, Y. Zheng, Removal of lead, copper, nickel, cobalt, and zinc from water by a cancrinite-type zeolite synthesized from fly ash, Chemical Engineering Journal. 145 (2009) 483–488.

[31] A. Dyer, J. Hriljac, N. Evans, I. Stokes, P. Rand, S. Kellet, R. Harjula, T. Moller, Z. Maher, R. Heatlie-Branson, J. Austin, S. Williamson-Owens, M. Higgins-Bos, K. Smith, L. O'Brien, N. Smith, N. Bryan, The use of columns of the zeolite clinoptilolite in the remediation of aqueous nuclear waste streams, J. Radioanal. Nucl. Chem. 318 (2018) 2473–2491.

[32] O. Halevi, T.Y. Chen, P.S. Lee, S. Magdassi, J.A. Hriljac, Nuclear wastewater decontamination by 3D-Printed hierarchical zeolite monoliths, RSC Adv. 10 (2020) 5766–5776.

[33] H. Schulz, P. Burtscher, L. Mädler, Correlating filler transparency with inorganic/polymer composite transparency, Compos. - A: Appl. Sci. Manuf. 38 (2007) 2451–2459.

[34] G.T. Whiting, A.D. Chowdhury, R. Oord, P. Paalanen, B.M. Weckhuysen, The curious case of zeolite–clay/binder interactions and their consequences for catalyst preparation, Faraday Discuss. 188 (2016) 369–386.

[35] K. Kennes, A. Kubarev, C. Demaret, L. Treps, O. Delpoux, M. Rivallan, E. Guillon, A. Méthivier, T. de Bruin, A. Gomez, B. Harbuzaru, M.B.J. Roeffaers, C. Chizallet, Multiscale Visualization and Quantification of the Effect of Binders on the Acidity of Shaped Zeolites, ACS Catal. (2022) 6794–6808.

[36] T. Babeva, R. Todorov, S. Mintova, T. Yovcheva, I. Naydenova, V. Toal, Optical properties of silica MFI doped acrylamide-based photopolymer, Journal of Optics A: Pure and Applied Optics. 11 (2009).

[37] L.B. Tunnicliffe, A.G. Thomas, J.J.C. Busfield, Light scattering and transmission studies of nanofiller particulate size, matrix cavitation, and high strain interfacial dewetting behavior in silica-elastomer composites, J Polym Sci B Polym Phys. 49 (2011) 1084–1092.

[38] R.M. Milton, Molecular sieve adsorbents, U.S, 1959.

[39] A.Y. Likhacheva, M.E. Malyshev, A.Y. Manakov, S. v. Goryainov, A.I. Ancharov, Non-hydrostatic compression of zeolite NaA in water medium: Connection to anomalous conductivity, Zeitschrift Fur Kristallographie. 224 (2009) 137–143.

[40] S.M. Mousavinasab, Effects of Filler Content on Mechanical and Optical Properties of Dental Composite Resins., in: Metal, Ceramic and Polymeric Composites for Various Uses, 1st ed, Rijeka, Croatia: In Tech, n.d.: pp. 421–428.

[41] M. Thommes, K. Kaneko, A. v. Neimark, J.P. Olivier, F. Rodriguez-Reinoso, J. Rouquerol, K.S.W. Sing, Physisorption of gases, with special reference to the evaluation of surface area and pore size distribution (IUPAC Technical Report), Pure and Applied Chemistry. 87 (2015) 1051–1069.

[42] M. Hong, L. Yu, Y. Wang, J. Zhang, Z. Chen, L. Dong, Q. Zan, R. Li, Heavy metal adsorption with zeolites: The role of hierarchical pore architecture, Chemical Engineering Journal. 359 (2019) 363–372.

[43] Y. Horikawa, N. Ohnishi, K. Hiraga, Structures and magnetic susceptibility of Ni-ion-introduced zeolite A and X, Materials Science and Engineering. (1996) 139–141.

[44] L.B. McCusker, K. Seff, Crystal structures of fully zinc(II)-exchanged zeolite A, hydrated and partially dehydrated at 600°C, Journal of Physical Chemistry. 85 (1981) 405–410.

[45] W. v Cruz, P.C. W Leung, K. Seff, Crystal Structures of Nitric Oxide and Nitrogen Dioxide Sorption Complexes of Partially Cobalt(II)-Exchanged Zeolite A, Inorg Chem. 18 (1979) 1692–1696.

[46] M.M. Eddy, A.K. Cheetham, Powder neutron diffraction study of zeolite Na-ZK-4; an application of new functions for peak shape and asymmetry, Zeolites. 6 (1986) 449–454.

[47] L.H. Allen, E. Matijević, Stability of colloidal silica: II. Ion exchange, J Colloid Interface Sci. 33 (1970) 420–429.

SUPPLEMENTARY INFORMATION

Table S1. Characteristics of LTA powder used in this work

Filler	Supplier	Si/Al	Ca/Al	Na/Al	Water content (wt %)	Crystal Size (D50, µm)	Bulk density ($g.cm^{-3}$)	Real density ($g.cm^{-3}$)
LTA-5A powder	ACROS ORGANICS	0.97	0.34	0.24	18	4.4	≥ 0.65 [a]	2.77

[a] Anten Chemical Co., Ltd.

Table S2. Formulations of different composites

Name of formulation	Zeolite (g)	Binder type	Binder (g)	Monomer (g)	BDMK (g)	Solid content
P-LTA	1.00	/	/	1.50	0.025	40 wt%
P-LTA-bentonite	1.00	powder	0.10	1.4	0.025	44 wt%
P-LTA-kaolin	1.00	powder	0.10	1.4	0.025	44 wt%
P-LTA-fumed silica	1.00	powder	0.10	1.4	0.025	44 wt%
P-LTA-montmorillonite	1.00	powder	0.10	1.4	0.025	44 wt%
P-LTA-lithopix P1	1.00	Sol. 50 wt%	0.20	1.30	0.025	44 wt%
P-LTA-waterglass	1.00	Sol. 27 wt%	0.35	1.25	0.025	44 wt%
P-LTA-10silica	1.00	Sol. 40 wt%	0.25	1.25	0.025	44 wt%
P-LTA-20silica	1.00	Sol. 40 wt%	0.50	1.00	0.025	48 wt%
P-LTA-30silica	1.00	Sol. 40 wt%	0.75	0.75	0.025	52 wt%

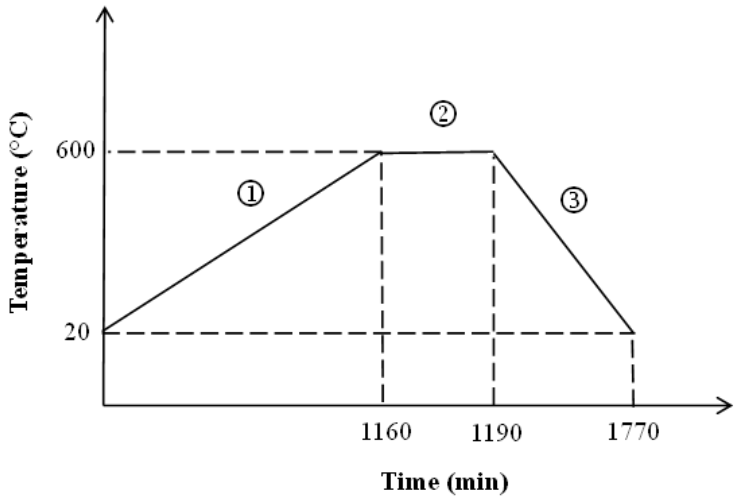

Figure S1. Temperature profile of thermal treatment process: ① ramp = 0.5 ℃/min; ② 600 ℃ for 30 min; ③ ramp = -1 ℃/min.

Figure S2. Compressive strength test for pellets after thermal treatment. (A) 100 g weight on LTA-10 dwb % silica; (B) 300 g weight on LTA-20 dwb % silica; (C) 300 g weight on LTA-30 dwb % silica. State 1: before test. State 2: pellet under weights. State 3: appearance of the pellet after test.

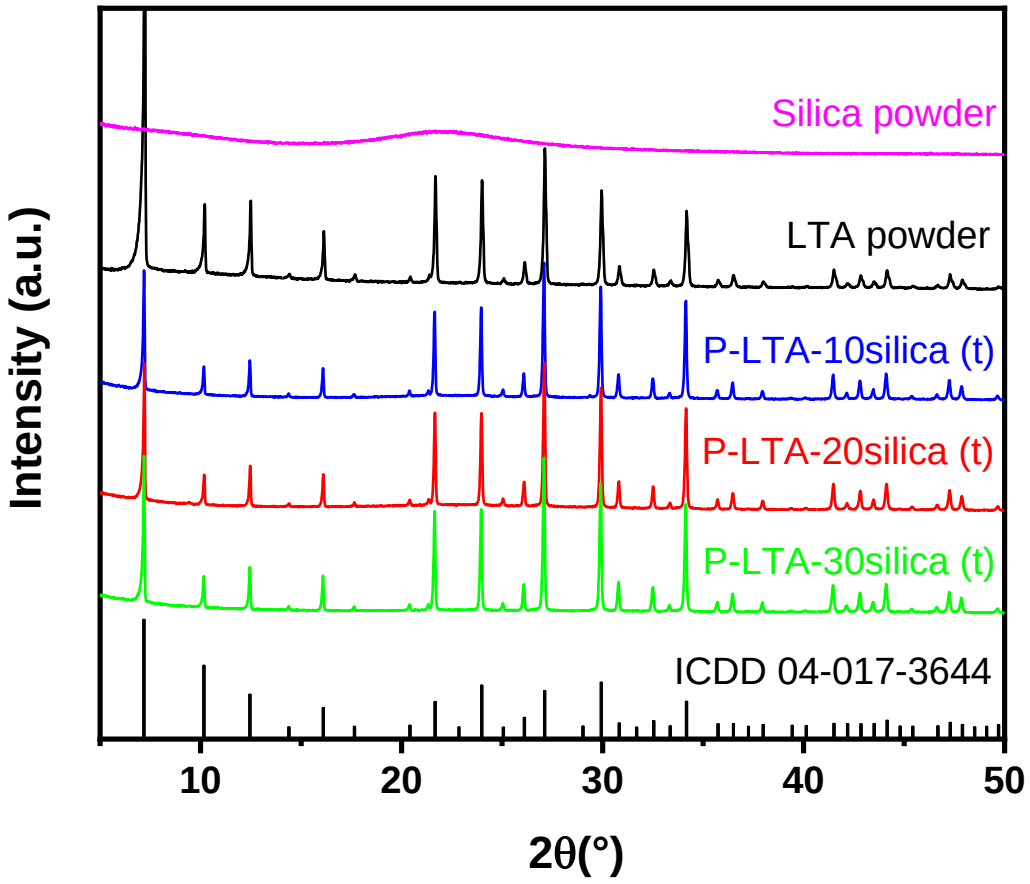

Figure S3. XRD patterns of Silica powder [a], LTA powder, P-LTA-10silica (t), P-LTA-20silica (t), P-LTA-30 silica (t) and reference pattern for LTA structure (ICDD 04-017-3644).

[a] Silica powder obtained by evaporation of water of Ludox HS-40 under 80 ^{o}C during one night.

Table S3. Lattice parameters and space groups for LTA powder and composites with different content of silica.

Sample	a=b=c (Å)	α=β=γ (°)	Space group	Cell volume (Å^3)
LTA-5A powder	12.3076(11)	90	Pm-3m	1864.3(3)
P-LTA-10silica (t)	12.3111(5)	90	Pm-3m	1865.89(14)
P-LTA-20silica (t)	12.3099(10)	90	Pm-3m	1865.4(3)
P-LTA-30silica (t)	12.3090(11)	90	Pm-3m	1865.0(3)

Table S4. Chemical analyses of cured PEGDA polymer matrix after Ni^{2+} and Sr^{2+} adsorption experiments

	Elements	Concentration (wt%)
Sr^{2+} adsorption	C	52.27
	O	47.37
	Al	0.01
	Si	0.02
	S	0.02
	Sr	0.31
Ni^{2+} adsorption	C	54.65
	O	45.00
	Al	0.02
	Si	0.03
	S	0.01
	Ni	0.29

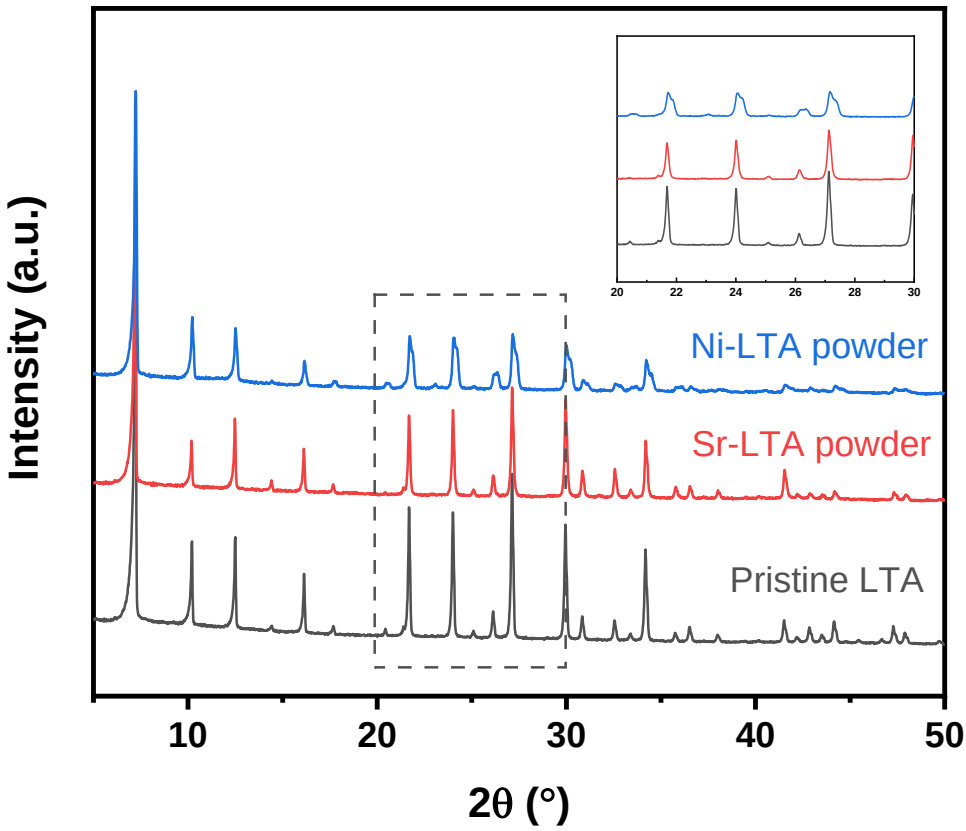

Figure S4. XRD patterns of LTA powder after 24 h exchange with Sr^{2+} and Ni^{2+}.

Table S5. Lattice parameters and space groups for LTA powder after 24 h exchange with Sr^{2+} and Ni^{2+}.

Sample	a=b=c (Å)	α=β=γ (°)	Space group	Cell volume ($Å^3$)
Pristine LTA	12.3076(11)	90	Pm-3m	1864.3(3)
Sr-LTA powder	12.2910(9)	90	Pm-3m	1856.78(25)
Ni-LTA powder	12.26705(6)	90	Pm-3m	1845.9528(3)

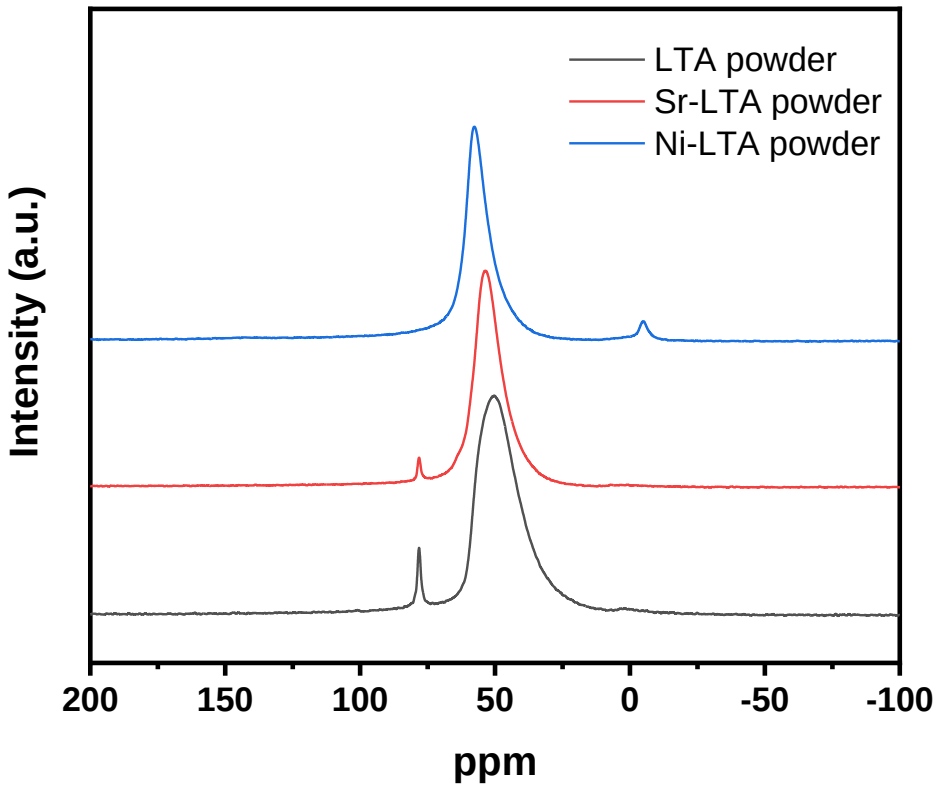

Figure S5. ^{27}Al NMR spectra of LTA powder (pristine powder), Ni-LTA powder (exchanged pristine powder) and Sr-LTA powder (exchanged pristine powder).

~76 ppm: residual $Al(OH)_4^-$ from industrial synthesis process; ~50 ppm: tetrahedral $Al(OSi)_4$; ~0 ppm: extra-framework aluminum.

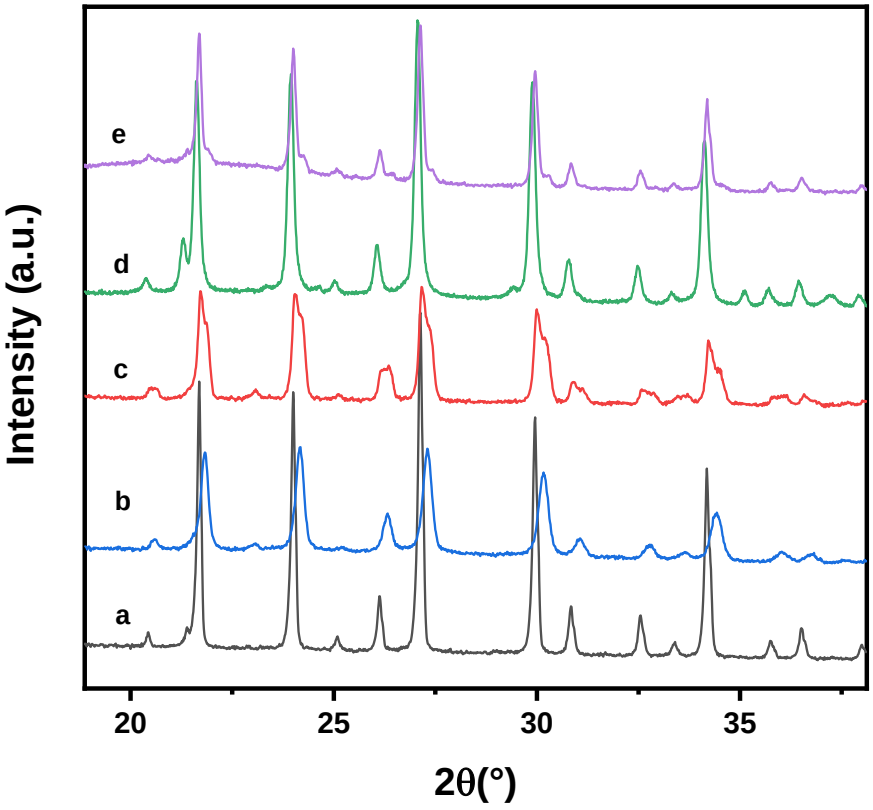

Figure S6. XRD patterns overlay of (a) LTA powder (pristine powder); (b) dealuminated LTA [a]; (c) LTA powder exchanged with Ni^{2+}; (d) P-LTA exchanged wit Ni^{2+} and (e) P-LTA-30silica exchanged with Ni^{2+}.

[a] LTA powder treated with 0.2M HCl under 80 °C for 3 hours.

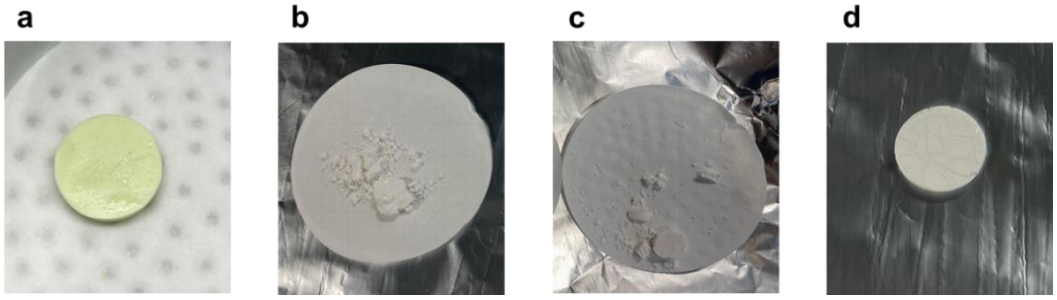

Figure S7. Monoliths after cation exchange of 24h at room temperature: (a) P-LTA-30silica (b) P-LTA (t), (c) P-LTA-20silica (t), (d) P-LTA-30silica (t).